JOURNAL OF PROPULSION AND POWER
Vol. 17, No. 4, July–August 2001

# Convergence Behavior of *Surface Evolver* Applied to a Generic Propellant-Management Device

Steven H. Collicott*
*Purdue University, West Lafayette, Indiana 47907-1282*

**Design of surface-tension propellant-management devices for acquisition and control of liquid propellants in weightless periods of space flight is a science with few analytical tools. One tool used increasingly is *Surface Evolver*. *Surface Evolver* can be used to solve the three-dimensional fluid statics problems necessary to characterize propellant-management device performance in weightlessness. Because of the interactive labor involved with running *Surface Evolver*, convergence and grid-size dependence issues can be expensive to explore for each tank and propellant-management device vane geometry. Results presented are of an investigation of convergence, grid-size dependence, consistency, and use of symmetry planes on *Surface Evolver* modeling of propellant distributions in a generic vane-type propellant-management device.**

## Nomenclature

| | | |
|---|---|---|
| $A$ | = | interface area |
| $k_1, k_2$ | = | principal curvatures |
| $P_L$ | = | pressure in liquid phase |
| $P_V$ | = | pressure in vapor phase |
| $R_{\text{av}}$ | = | scalar measure of sphericity |
| $r_t$ | = | tank radius |
| $V$ | = | vapor volume |
| $x$ | = | transverse coordinate |
| $y$ | = | transverse coordinate |
| $z$ | = | axial coordinate |
| $\sigma$ | = | surface tension |

## I. Introduction

THE static geometry of liquid distribution in a propellant-management device (PMD) is a three-dimensional problem because of the various vanes, sponges, arms, and other components used to control the liquid propellants in weightlessness.[1] *Surface Evolver*[2] can be used to solve the three-dimensional fluid statics problems necessary to characterize PMD performance. *Surface Evolver* has been used to model several different low Bond-number fluids issues in spacecraft.[3–6] Experiments by the author and colleagues[7,8] and others[5] have verified that *Surface Evolver* can be used to model small Bond-number fluid statics geometries. The lack of cost of *Surface Evolver* and its availability in Unix, personal computer (DOS, Windows, and Linux), and MacIntosh versions strengthen its appeal.

The static fluid interface geometry is most often discussed with reference to the relation between the sum of the principal curvatures and the uniform pressure jump across the liquid–vapor interface, $P_V - P_L = \sigma(k_1 + k_2)$. However, the problem is solved in *Surface Evolver* by minimizing the energy of the system. The energies in the system are defined by the specifications in the initial geometry file, such as in Appendices A and B.

Convergence of *Surface Evolver* to a final solution is of course important, yet it is often difficult to judge, especially for the less experienced user. The impact of the fineness of the faceting (grid size) is similarly important to producing relevant output. The use of symmetry plane constraints is an attractive method to reduce computational time. Assurance that a segment of the tank model converges well and represents the full-tank problem can be important in justifying one's methods and predictions. These three tasks are studied in a representative geometry with a range of vapor volumes. The results are presented with a variety of comparisons. Implications of the results are then discussed.

## II. Tank and PMD

A cylindrical tank with four straight vanes on the perimeter is modeled. A cross-section is shown in Fig. 1. Measurements of the axial length of the vapor bubble solution for a range of vapor volumes are useful for design of the end-cap regions of the PMD. Thus, the endless tank model provides valuable empirical data to aid in PMD design in addition to the principal purposes (convergence, grid, and symmetry evaluations). Straight vanes on the outer wall are used, for example, in the cylindrical section of the hydrazine tank in the Lockheed Martin A2100 series of geosynchronous commercial communications satellites. Vanes in cylindrical and spherical tanks historically have not been attached to the tank walls but separated by a small gap. In the present model, these small gaps are always submerged in the liquid propellant and the vane is of zero thickness, so the gap itself need not be modeled.

The radius of the tank interior is set to unity. Contact angle is chosen to be 0 deg, representative of the familiar hydrazine on titanium problem. The four vanes begin at the outer wall, and extend inward to $r = 0.75$. Vapor volumes are thus nondimensionalized by tank radius cubed, and surface areas by tank radius squared. The magnitude of the surface tension is irrelevant because the only energy in this isothermal 0 $g$ fluid statics problem is surface energy, which is the product of surface area and surface tension. Similarly, pressure of the gas in the bubble does not affect the solution of the static liquid–vapor interface. Increasing gas pressure uniformly increases liquid pressure, so the pressure difference across the curved interface, and the interface shape itself, remain unchanged. Temperature gradients will create thermal capillary convection and perhaps phase-change mass transfer, which can not be modeled in *Surface Evolver*. However, nothing else can provide the high-resolution solutions of the three-dimensional free surface (the hydrazine and helium interface), and so *Surface Evolver* is a unique and valuable tool for PMD design.

## III. Starting Geometry

There are two starting geometries for the *Surface Evolver* computations in this research. One is a stretched cube with one pair of opposite vertices coincident with the tank axis, as shown in Fig. 2. For the symmetry evaluation exercise, one-eighth of the full-tank starting geometry is used. There are two facets in the one-eighth-tank model starting geometry (Fig. 3.) The tank axis is vertical in Fig. 3, as are the lines showing the inner and outer extent of the straight vane. In both cases, the $z = 0$ plane is at the tank equator

Presented as Paper 99-0846 at the 37th Aerospace Sciences Meeting and Exhibit, Reno, NV, 11–14 January 1999; received 5 December 1999; revision received 18 January 2001; accepted for publication 27 January 2001. 

*Associate Professor, School of Aeronautics and Astronautics. Senior Member AIAA.

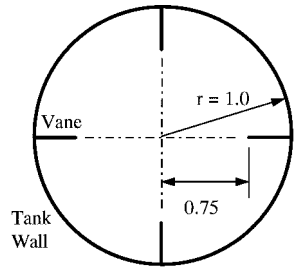


**Fig. 1 Cross-section of endless tank model. Hydrazine wets the tank wall and vane surfaces at approximately 0 deg contact angle. Vanes hold the helium bubble in the center and hold small fillets of fuel near satellite end-of-life.**

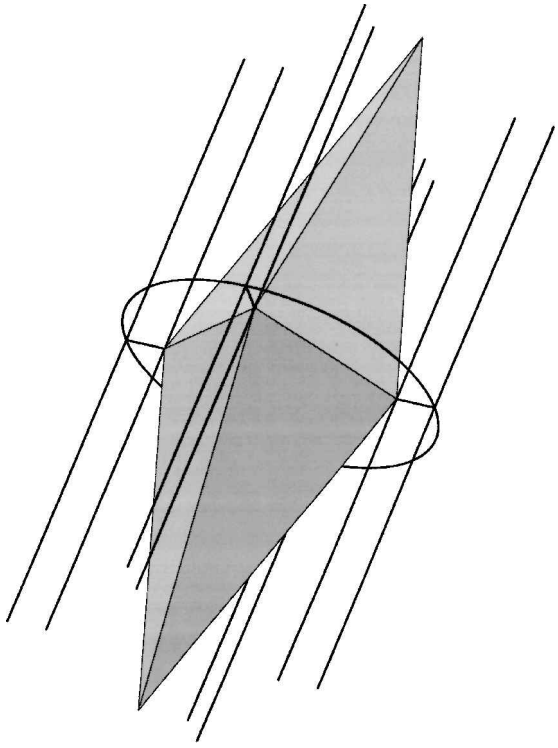

**Fig. 2 Starting geometry for full-tank model. All computed volumes with all numbers of facets begin from this geometry. Straight, parallel lines show vane inner and outer (tank wall) edges over an axial distance of $4r_t$.**

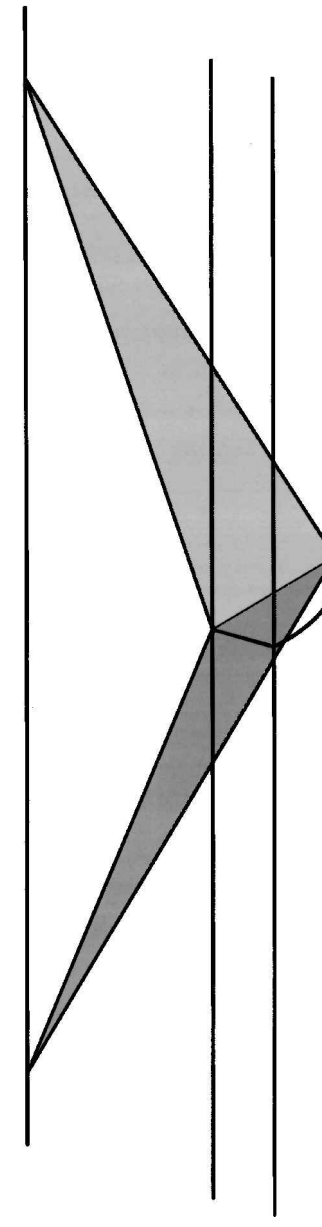

**Fig. 3 Starting geometry for one-eighth tank model. All computed volumes with all numbers of facets begin from this geometry. Straight, parallel lines show vane inner and outer (tank wall) edges over an axial distance of $4r_t$.**

and normal to the tank axis of symmetry. Symmetry about the equatorial plane is not exploited because the PMD vane geometry usually differs between the outlet and vent ends of the tank. Example *Surface Evolver* geometry definition files for these two cases are shown in Appendices A and B.

## IV. Diagnostics

The *Surface Evolver* manual[2] is the fundamental source for advice on running the code. In the runs performed in this exercise, experience is acquired, leading to specific advice on running *Surface Evolver* effectively in this type of geometry. This advice is consistent with the advice given in the manual, yet with a magnitude spelled out. For example, when minimum and maximum facet areas are maintained within the same order of magnitude, performance is reliable. Within a factor of four or five, performance is superior. Similar bounds for the magnitude ratio on edge lengths, enforced simultaneously, are helpful for producing the best performance. Areas and lengths are monitored in this work with the histogram command: For example, histogram (face, area) for the areas and histogram (edge where not fixed, length) for the edges defining the bubble, but not the edges used to draw the tank and vane outlines.

Convergence is assessed by the energy of the solution, in this case just surface area. An absolute measure is not possible because an analytical solution is not found for this, and most other economically important, geometries. However, comparison to the convergence of *Surface Evolver* in the tank and PMD geometry to a well-behaved case (a faceted sphere) can be made. As shown in the following, the faceted sphere case compares favorably to characteristics of the two regular solids with the most faces.

In a typical PMD geometry, it cannot be determined that the solution has reached the global minimum in energy. A local minimum can be evaluated to some extent by "jiggling" the solution (j command in *Surface Evolver*), but fundamentally one cannot tell the difference between a deep local minimum and the global minimum. One check is to shrink the bubble axially, to see if the bubble converges again to the same point. This is repeated with axial stretching. This process also determines the length that a bubble of a given volume will be in vanes of this type, which provides useful data for evaluating PMD performance at different fill fractions.

Comparisons between grid-size cases show expected behavior: More facets are a better representation of a curved surface, thus the total surface area is smaller for the same volume. Convergence of more facets requires more iteration, as mentioned in the *Surface Evolver* manual. Intermediate stages of the solution sometimes converge to the point where no more change appears possible. Jiggling (j), vertex averaging (V), equi-angulation (u), trimming (t), and weeding (w) or refining the faceting to keep the area and length ranges small can each get the solution out of the local minimum and toward a lower-energy solution. Hence, the local nature of the minimum is recognized only after the fact. Note that to produce

data for this research that are most consistent and most easily compared between volumes, commands that remove components from the model (weeding and trimming, for example) are not used in the evolution of solutions reported in this paper.

Comparison of the area and convergence of the one-eighth-tank solution with the full-tank solution evaluates the use of symmetry. Vertices on constraints, such as the symmetry planes (constraints 1 and 2 in Appendix B, for example) must remain in those planes, but in the full-tank model the facets and edges are free to span such planes. Thus the vertices and edges in symmetry planes lack 1 degree of freedom. The impact of this additional constraint on the minimization algorithms of *Surface Evolver* in this geometry is hoped to be small and is tested in this work. With these differences in mind, this question is posed: How well does use of one-eighth of the tank to save time produce the same surface solution?

Comparison between different volumes and numbers of facets is performed concisely by computing the (nondimensional) ratio of surface area, $A$, to the two-thirds power of volume, $V$. This ratio is referenced to that for a sphere, for the sphere is, of course, the solution with minimum surface area per volume, $(36\pi)^{1/3}$:

$$R_{\text{av}} = \text{AV}^{-\frac{2}{3}} \Big/ (36\pi)^{\frac{1}{3}} \tag{1}$$

A perfect sphere, then, will produce $R_{\text{av}} = 1$, so the difference $(R_{\text{av}} - 1)$ is the fractional change in $(\text{AV}^{-2/3})$ relative to a sphere.

Another comparison for each volume can be made between the computed $R_{\text{av}}$ and the value computed for a prolate spheroid of semiminor axis equal to the tank radius and with a volume equal to the helium volume. The prolate spheroid is, of course, not a solution for the interface but rather is a simple and fundamental check on the magnitude of $R_{\text{av}}$ for the actual solutions. Comparisons at constant volume can be made with bubble length and equatorial circumference. The shape and thickness of the "fillet" of fuel wicked into the vane–tank intersection is of use in estimations made in PMD design.

## V. Results

### A. Shape Versus Volume

Figures 4, 5, and 6 show example solutions for 512 facets on the full-tank model for helium volumes of $3r_t^3$, $10r_t^3$, and $30r_t^3$, respectively. Performance of the full-tank model of up to 32,768 facets is presented below, but the 512-facet models reproduce most clearly in the present format. Figure 7 shows the $V = 6r_t^3$ solution with the surface of 8192 facets rendered in stripes of gray for radial contours in steps of $0.1r_t$. The $V = 30r_t^3$ solution looks like the $V = 10r_t^3$ solution with the equatorial region stretched out axially. This observation is confirmed with comparisons of bubble lengths versus bubble volume.

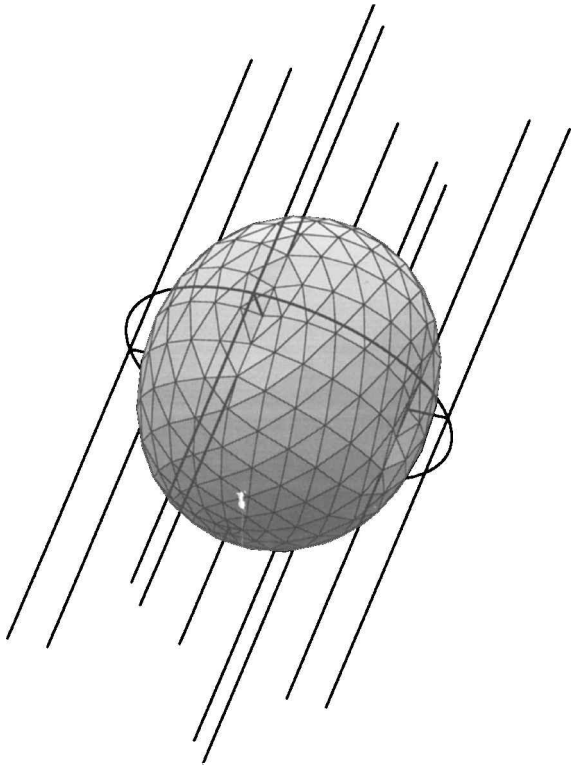

**Fig. 4 Typical full-tank solution for a volume of $3r_t^3$.**

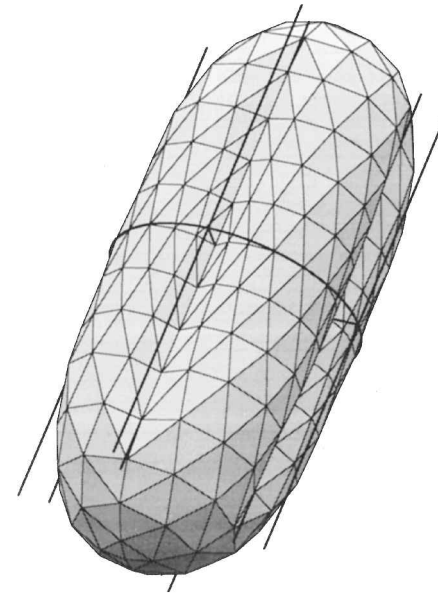

**Fig. 5 Typical full-tank solution for a volume of $10r_t^3$ and 512 facets.**

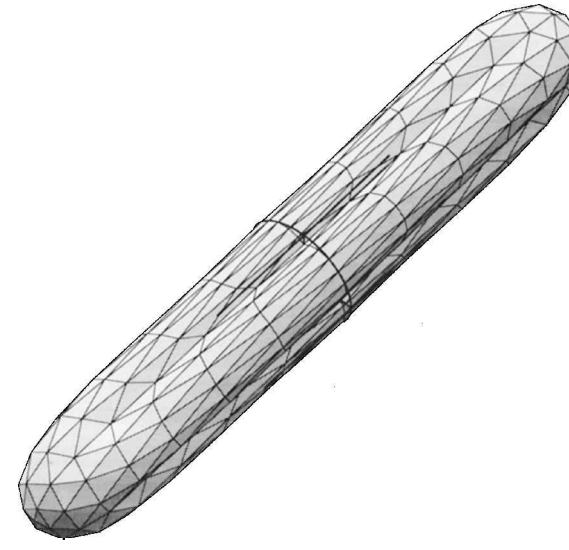

**Fig. 6 Typical full-tank solution for a volume of $30r_t^3$ and 512 facets.**

Comparing Figs. 4 through 7 shows the increasingly large area of contact between the interface and the tank wall with increasing volume. The $V = 6r_t^3$ case shows a sizable area of the interface within $0.1r_t$ distance of the wall. In contrast, Fig. 4 shows clearly that the interface for that vapor volume does not impinge at all on the tank wall, as shown by the equator.

The equatorial cross-sections of various facetings and volumes are presented in Fig. 8. Note in the upper- and lower-right quadrants of Fig. 8 that the $V = 30r_t^3$ bubble does not impinge on the tank wall as much as the $V = 10r_t^3$ bubble does, even with 2048 facets on the large bubble. One would expect the larger-volume bubble to impinge on the wall to a greater, not lesser, extent. This paradox is likely a result of the more slender facets near the equator of the larger bubble, as shown in Fig. 6 (for the 512-facet case), forced into representing a larger surface area on the interface than on the smaller volume bubble.

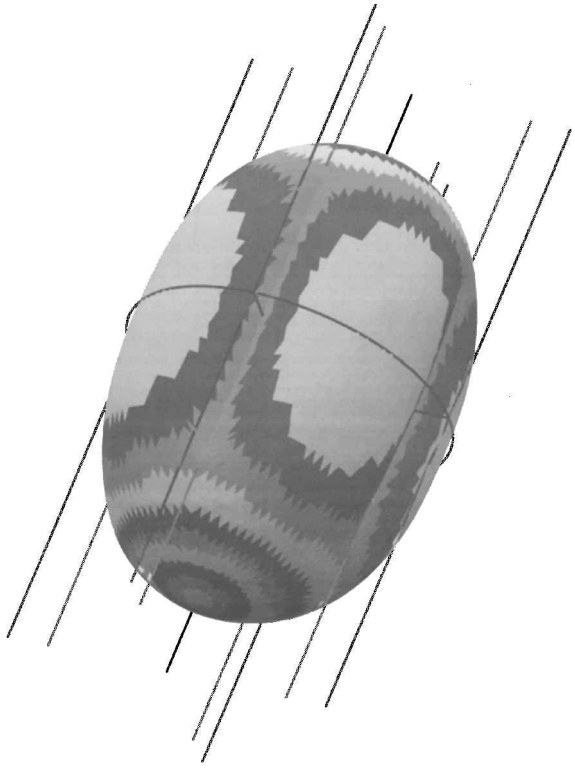

**Fig. 7 $V = 6r_t^3$ bubble with 8192 faces and stripes every step of $0.1r_t$ radial distance from the axis.**

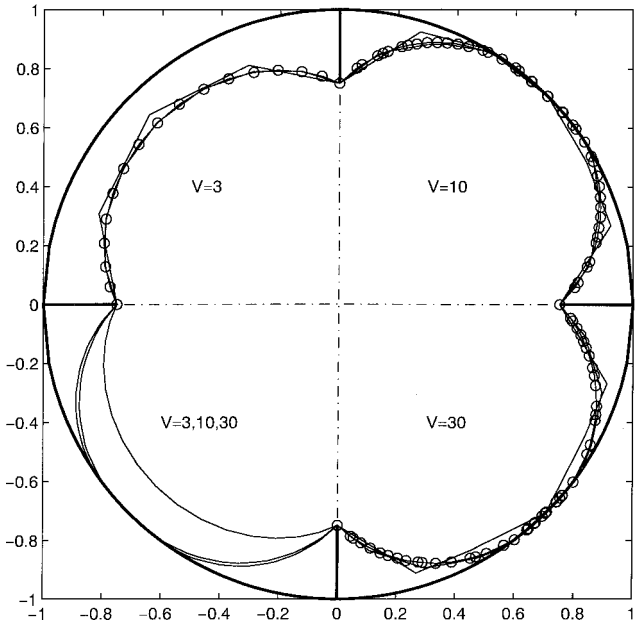


**Fig. 8 Plots of equatorial shapes for various volumes and facetings. One-quarter of the tank cross-section is shown for four examples. Clockwise from upper left: 128-, 512-, and 2048-facet solutions for $V = 3r_t^3$, $V = 10r_t^3$, and $V = 30r_t^3$, and the 2048-facet solutions for all three volumes.**

The axial length of the solutions are of interest in assessing consistency of solutions for a range of volumes and for use in estimation of when tank end caps become important to bubble shape. Results of a study of bubble length versus volume are presented in Fig. 9 (solid line marked by circles). The same measure for a sphere is diameter, and this is plotted as the unmarked solid curve through the origin. The nearly linear behavior of bubble length versus volume at volumes greater than four or five shows that as volume is increased, the bubbles mostly elongate rather than push farther into the vane–wall intersection. This can also be seen by comparing the $V = 10r_t^3$ and $30r_t^3$ results in the lower-left quadrant of Fig. 8. The smoothness of the bubble area versus volume curve is an indication of the consistency of the solutions. The manner in which the data meet the area versus volume data of spheres (dashed curve through the origin) at $(V/r_t^3) = 1.77$ verifies the accuracy of the method.

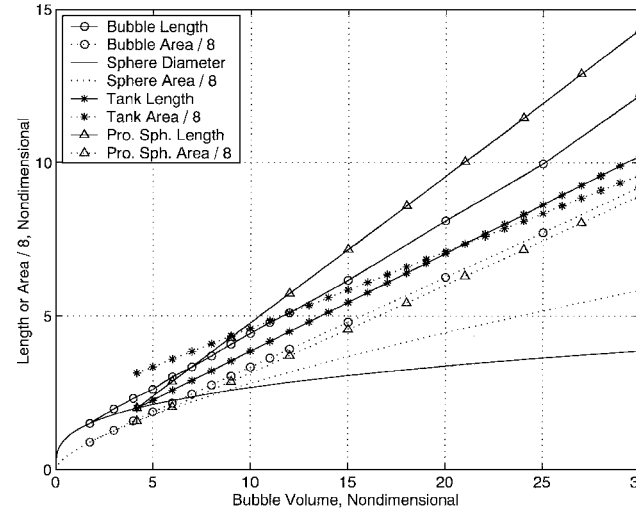


**Fig. 9 Bubble length and one-eighth area versus bubble volume with comparison with a sphere, a cylinder-hemisphere tank, and a prolate spheroid. One-eighth areas are plotted to fit on the same scale as the lengths.**

Two other pairs of curves in Fig. 9 are the length and one-eighth-area results for a cylindrical tank with hemisphere ends (asterisks) and for a prolate spheroid with a semiminor axis equal to unity (triangles). These geometries are relevant for nondimensional volumes above $4\pi/3$. The similarity of the bubble area to the prolate spheroid area is remarkable, although there are substantial differences in the lengths.

### B. Grid Convergence

Figure 10 presents the resulting area–volume relation, defined in Eq. (1), for solutions spanning one order of magnitude in volume and three orders in numbers of facets. The bottom, central, and top groups of data are volumes of $3r_t^3$, $10r_t^3$, and $30r_t^3$, respectively. Circles connected with solid lines mark data for the full-tank model. Star symbols with solid lines mark the one-eighth-tank results. Comparing these two lines shows the efficiency of the one-eighth-tank method. Far fewer facets, and hence less iteration and less elapsed time, are required to approach a given limit to within a given discretization error.

The dashed line with $x$ marks in each group is the one-eighth-tank data shifted right to eight times the number of facets used on that one sector. Comparing this line with the full-tank results shows the relative effectiveness of the one-eighth-tank model and the full-tank model at representing the surface with the same number of facets over the entire surface (or same number of facets per unit area of the interface).

Consider first the results for the fully faceted unconstrained sphere, shown as the solid line with circles near the lower-left corner of Fig. 10. The slope of the lines for sphere data is −1, showing that discretization error depends inversely on the number of facets. That the sphere line is steep compared with the other lines is not an issue: $(R_{\text{av}} - 1)$ must go to zero for an infinite number of facets on the sphere, but must not tend to zero for the elongated and creased geometries of the larger bubble volumes.

The two dashed-dotted lines in Fig. 10 are the $R_{\text{av}}$ values for prolate spheroids for $V = 10r_t^3$ and $30r_t^3$. The respective line for a $V = 3r_t^3$ prolate spheroid is below the bottom of the plot. Comparison with the prolate spheroid is not expected to be exact, but rather is useful for understanding the magnitudes of the results.

The upper-left end of the sphere line is near two diamond symbols. These represent the value of $R_{\text{av}}$ for the two regular solids with the most faces, the dodecahedron (12 pentagons) and the icosahedron

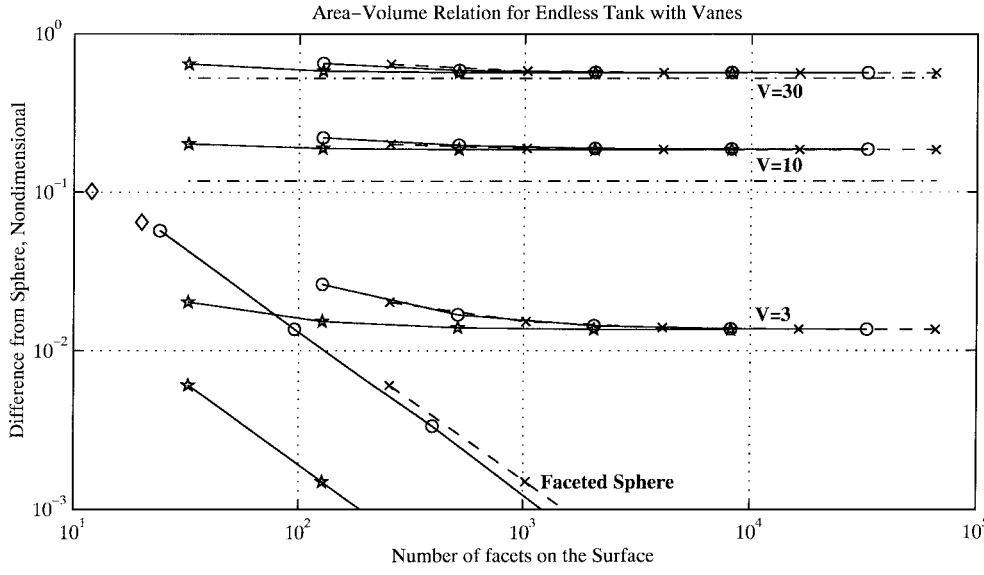


**Fig. 10 Plot of area–volume relation versus numbers of facets for helium bubbles of three volumes. The two diamond symbols at the left are computed from the regular solids dodecahedron (12 pentagons) and icosahedron (20 triangles).**

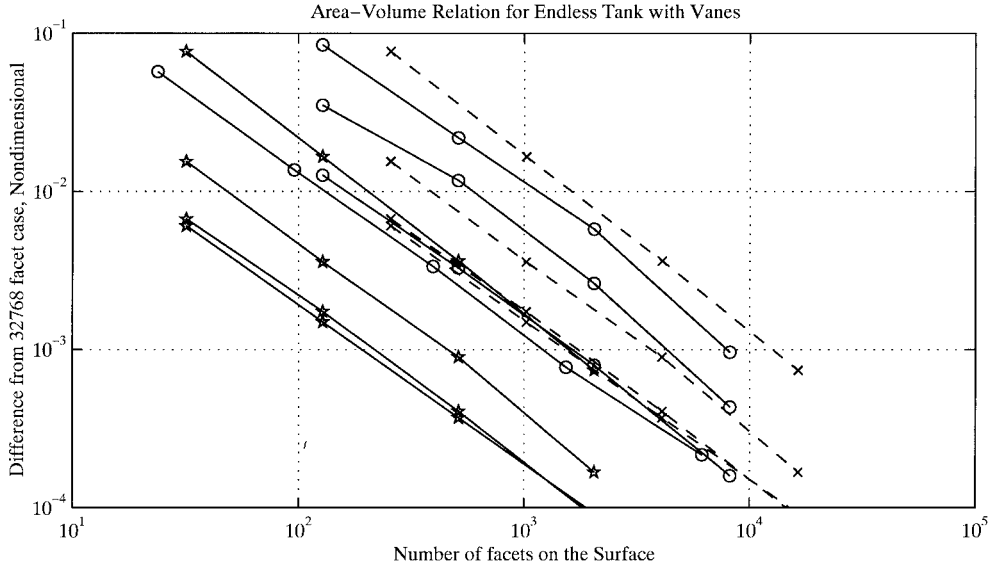


**Fig. 11 Plot of the difference between the area–volume relation and the value for 32,768 facets.**

(20 triangles). Note that the $R_{av}$ data for regular solids are consistent with the data for the unconstrained sphere calculations in *Surface Evolver*. This is a validation, by two fundamental solids, of the calculations presented here for the sphere. Thus the sphere data are used with confidence to assess the characteristics of the bubble constrained by the PMD vanes.

Comparison of the $3r_t^3$ bubble results in Fig. 10 to those for the sphere shows that this small-volume bubble is nearly spherical. That is, for large numbers of facets, $R_{av}$ approaches 1.01. Thus the helium–hydrazine interface is creased only slightly by impingement on the vanes. This is apparent in the equatorial shape (upper-left quadrant in Fig. 8) and in a picture of a typical result for this volume (Fig. 4). Note that the volume of the sphere that would be tangent with the inner edges of the vanes is $V = (4\pi/3)(0.75r_t)^3 \approx 1.77r_t^3$, and a sphere of volume $3r_t^3$ has a radius of approximately $0.9r_t$. The next largest volume, $V = 10r_t^3$, (upper-right quadrant of Fig. 8) shows substantial creasing of the interface by the vane. At this volume, the interface impinges on the outer wall of the tank, unlike the $V = 3r_t^3$ case.

Although Fig. 10 illustrates how well the faceted sphere converges to the perfect sphere with increasing numbers of facets, those data are difficult to view in the curves for the nonspherical bubbles. Figure 11 provides a better view of the grid dependence of the nonspherical bubbles. This figure shows the difference between the $R_{av}$ values for each volume and the value of $R_{av}$ computed for the solution for that volume using the greatest number of facets (typically 32,768 facets). Now the spherelike grid convergence is evident for all three bubbles for both full-tank models and one-eighth-tank models.

Thus all solutions are shown to have spherelike grid convergence, and the sphere is shown at the coarsely faceted limit to be consistent with regular solids. The sphere results also show that error tends toward zero inversely with number of facets. A lesson from elementary calculus is sufficient to caution that the error for the sphere cannot go to zero for any finite number of facets, and it is reasonable to apply this to the nonspherical solutions too.

### C. Perturbations

One method to assess how close a solution is to the very bottom of an energy minimum is to perturb the solution and examine the response. The solution may move to a deeper minimum, or it may reconverge to the original minimum. As a illustration, a one-eighth-tank solution for a $V = 11r_t^3$ bubble is stretched in length by 10%. The *Surface Evolver* command for use with solutions from the starting geometries in Appendices A and B is set vertex z z*1.1.

Figure 12 shows the response of the length and the surface energy of the one-eighth-tank $V = 11r_t^3$ bubble solution to the 10% elongation. Note that the energy very quickly drops back to essentially the original energy, whereas the bubble length decreases slowly. The bubble length ends up smaller than before. The energy is about 1 part in 30,000 below the original energy. Thus the bubble is in a fairly flat minimum with respect to bubble length; $\partial(\text{energy})/\partial(\text{length}) \ll (\text{energy}/\text{length})$. The apparent presence of two or more (timelike) scales in the length versus iteration curve is not understood at present.

Figure 13 shows results for bubble length reconvergence trends for solutions from 32 to 32,768 facets after a 10% stretching of a $V = 3r_t^3$ bubble. Solid lines show data for complete solution and dashed lines show the response of the one-eighth-tank solution. The analogous curves for reconvergence of energy are all approximately 1 decade to the left of the length curves, as typified by the pair of curves in Fig. 12. Curves for volumes of $V = 10r_t^3$ and $30r_t^3$ lie in the same range as the $V = 3r_t^3$ curves. As expected, within the band of data in the figure, solutions with fewer facets reconverge more quickly. Differences between one-eighth- and full-tank models with the same number of facets are expected because the one-eighth will be a higher-fidelity model encompassing a wider range of length scales for curvature of the interface. When one-eighth- and full-tank data are compared based on equal number of facets per unit surface area, the reconvergence performance of the one-eighth-tank model appears only slightly superior.

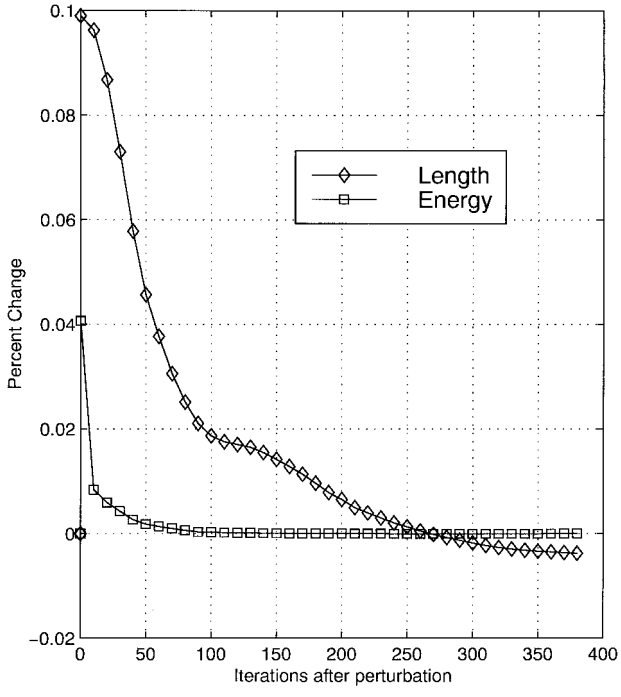


**Fig. 12 Response of the one-eighth tank $V = 11r_t^3$ bubble solution to a 10% length increase perturbation.**

## VI. Conclusions

In the geometry of the cylindrical tank with perimeter vanes, no analytical solution is known with which to directly measure the effects of grid refinement on absolute error. However, the decrease of relative error with increasing number of facets for the vaned-tank solutions mimics that of the faceted unconstrained sphere. The sphere has an analytical solution and, through comparison to the regular solids, the sphere solutions produce a fundamental validation of the error measure chosen for this work. The conclusions are, then, that a doubling of facets halves the error due to the grid and no finite number of facets results in zero error.

Exploiting symmetry of the tank and PMD geometry can produce substantial time savings for a given error, or substantial error reduction for a given elapsed computational time. The data for the unconstrained sphere show an eightfold reduction in error for a given number of facets on one-eighth of the sphere rather than on the whole sphere. When compared as error per unit of surface area, the one-eighth-sphere model is very slightly worse than the full-sphere model. (The dashed line in the lower left of Fig. 10 is slightly above the solid line with circles.) However, the one-eighth model would then have 16.3% of the facets of the full sphere rather than just 12.5%, so the time savings remain substantial.

A study of the response of a solution to perturbations indicates that energy reconverges more quickly than the axial length of the bubble does. This shows that it is useful to monitor several quantities when applying *Surface Evolver* to PMD design tasks. Another study

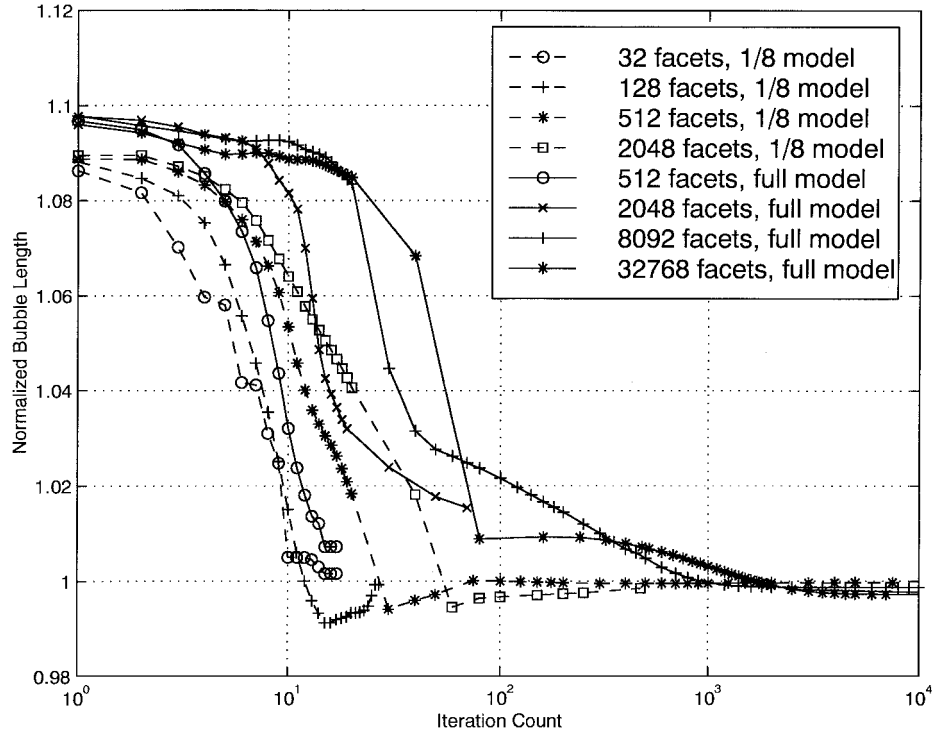


**Fig. 13 Response of numerous $V = 3r_t^3$ bubble solutions to a 10% length increase perturbation.**

shows that the relations of axial length and surface energy to bubble volume are consistent and agree nicely with those for a sphere.

The research results presented here are quantitative benchmarks to aid industry in applying *Surface Evolver* to tank and PMD geometries. Comparisons between tank and sphere and between tank and prolate-spheroid estimates show that the *Surface Evolver* models are performing in a reasonable manner. More facets are always better, and exploiting symmetry leads to time reductions with but a minimal, and recoverable, impact on error.

## Appendix A: Full-Tank Starting Geometry

```
// Endless tank Surface Evolver model,
// Steven H. Collicott
// collicot@ecn.purdue.edu
// Tank radius = 1.
// Nondimensional quantities.
#define srftns 1
#define massdensity 1
Constraint 1     // Vane plane.
Formula: x = 0
Constraint 2     // Vane plane.
Formula: y = 0
Constraint 3 nonnegative      // x-vanes.
Formula: 0.75 - abs(x) = 0
Constraint 4 nonnegative      // y-vanes
Formula: 0.75 - abs(y) = 0
Constraint 5 nonnegative      // In tank.
Formula: 1 - (y^2 + x^2) = 0
Constraint 6                  // Tank wall.
Formula: 1 - (y^2 + x^2) = 0

Vertices
1    0       0    -1 constraints 1, 2
2    0       0.75  0 constraints 1, 4
3    0       0     1 constraints 1, 2
4    0.75    0     0 constraints 2, 3
5    0      -0.75  0 constraints 1, 4
6   -0.75    0     0 constraints 2, 3
Edges
1   1  2  constraints 1, 4
2   2  3  constraints 1, 4
3   1  4  constraints 2, 3
4   4  3  constraints 2, 3
5   1  5  constraints 1, 4
6   5  3  constraints 1, 4
7   1  6  constraints 2, 3
8   6  3  constraints 2, 3
9   2  4  constraints 5
10  4  5  constraints 5
11  5  6  constraints 5
12  6  2  constraints 5
Faces
1    1    9    -3 constraint 5 tension srftns
2    7    12   -1 constraint 5 tension srftns
3    11   -7    5 constraint 5 tension srftns
4    3    10   -5 constraint 5 tension srftns
5   -9    2    -4 constraint 5 tension srftns
6   -12   8    -2 constraint 5 tension srftns
7   -11   6    -8 constraint 5 tension srftns
8   -10   4    -6 constraint 5 tension srftns
Body
1 1 2 3 4 5 6 7 8 volume 10
```

## Appendix B: One-Eighth-Tank Starting Geometry

```
// one-eighth endless tank Surface Evolver model,
// Steven H. Collicott
// collicot@ecn.purdue.edu
// Tank radius = 1.
// Nondimensional throughout.
#define srftns 1
#define massdensity 1
Constraint 1     // One bounding plane.
Formula: y = 0
Constraint 2     // One bounding plane.
Formula: y = x
Constraint 3 nonnegative     // x - vanes.
Formula: 0.75 - x = 0
Constraint 4 nonnegative     // In tank.
Formula: 1 - (y^2 + x^2) = 0
Constraint 5                 // Wall of tank.
Formula: 1 - (y^2 + x^2) = 0
// One-sided x-plane constraint
Constraint 6 nonnegative
Formula: y = 0
// One-sided x = y plane
Constraint 7 nonnegative
Formula: x = y
Vertices
1   0      0     -1  constraints 1, 2
2   0.75   0.75   0  constraints 2, 4
3   0      0      1  constraints 1, 2
4   0.75   0      0  constraints 1, 3
Edges
1 1 2   constraints 2, 4
2 2 4   constraints 4, 6, 7
3 1 4   constraints 1, 3
4 3 2   constraints 2, 4
5 3 4   constraints 1, 3
Faces
1 1  2 -3 constraint 4 tension srftns
2 5 -2 -4 constraint 4 tension srftns

Body
1 1 2 volume 1.125 // Vol = 1/8 of total.
```

## Acknowledgments

The financial assistance of the Lockheed Martin Missiles and Space Company, Sunnyvale, CA, and the support of aerospace engineering education by Jack Divers and Setrige Crawford of the Propulsion, Thermal, and Ordnance Product Center are appreciated. The author was on sabbatical working on commercial space products at the Lockheed Martin Missiles and Space Company when the bulk of the work reported was performed. This enthusiastic support of aerospace engineering education shown by Jack Divers and Setrige Crawford of the Propulsion, Thermal, and Ordnance Product Center and the financial assistance of the Lockheed Martin Missiles and Space Company are appreciated.

## References

[1]Rollins, J. R., Grove, R. K., and Jeakle, D. E., Jr., "Twenty-three Years of Surface Tension Propellant Management System Design, Development, Manufacture, Test, and Operation," *Proceedings of the AIAA 21st Joint Propulsion Conference*, AIAA Paper 85-1199, AIAA, Washington, DC, 1985.

[2]Brakke, K. A., *Surface Evolver*. Manual and code available at http://www.geom.umn.edu.

[3]Bayt, R. L., and Collicott, S. H., "Effects of an Elliptic End-Cap on the Ullage Bubble Stability in the Gravity Probe-B Satellite," *34th AIAA Aerospace Sciences Meeting*, AIAA Paper 96-0596, AIAA, Washington, DC, Jan. 1996.

[4]Bayt, R. L., "End Cap Effects on Vapor Bubble Stability in the Gravity Probe-B Main Helium Tank," Master's Thesis, School of Aeronautics and Astronautics, Purdue University, West Lafayette, IN, Aug. 1995.

[5]Dominick, S., and Tegart, J., "Orbital Tests Results of a Vaned Liquid Acquisition Device," *30th AIAA/ASME/SAE/ASEE Joint Propulsion Conference*, AIAA Paper 94-3027, AIAA, Washington, DC, July 1994.

[6]Tegart, J., "A Vane-Type Propellant Management Device," *33rd AIAA/ASME/SAE/ASEE Joint Propulsion Conference*, AIAA Paper 97–3028, AIAA, Washington, DC, July 1997.

[7]Collicott, S. H., Bayt, R. L., and Courtney, S. D., "Ullage Bubble Stability in the Gravity Probe-B Helium Tank," *30th AIAA Joint Propulsion Conference*, AIAA Paper 94-3026, AIAA, Washington, DC, June 1994.

[8]Krautheim, M. S., "One-g Fluid Experiments in the Gravity Probe-B Main Helium Tank," *34th AIAA Aerospace Sciences Meeting*, AIAA Paper 96-0006, AIAA, Washington, DC, Jan. 1996.